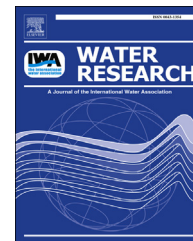


Available online at www.sciencedirect.com

ScienceDirect

journal homepage: www.elsevier.com/locate/watres

Effects of molecular weight-dependent physicochemical heterogeneity of natural organic matter on the aggregation of fullerene nanoparticles in mono- and di-valent electrolyte solutions

Mo-Hai Shen^a, Yong-Guang Yin^a, Andy Booth^b, Jing-Fu Liu^{a,*}

^a State Key Laboratory of Environmental Chemistry and Ecotoxicology, Research Center for Eco-Environmental Sciences, Chinese Academy of Sciences, Beijing, 100085, China

^b SINTEF Materials and Chemistry, Trondheim, NO-7465, Norway

ARTICLE INFO

Article history:

Received 12 June 2014

Received in revised form

10 December 2014

Accepted 14 December 2014

Available online 5 January 2015

Keywords:

Natural organic matter (NOM)

Molecular weight (MW)

Fullerene nanoparticles (nC₆₀)

Aggregation

Electrolytes

ABSTRACT

Given the wide presence of heterogeneous natural organic matter (NOM) and metal ions (Na⁺/Ca²⁺/Mg²⁺), as well as their significant role in governing nanoparticle stability in aqueous environments, it is of great importance to understand how the molecular weight (MW)-dependent physicochemical properties of NOM impact fundamental transportation processes like the aggregation of engineered nanoparticles (ENPs) in the presence of Na⁺/Ca²⁺/Mg²⁺. Here, we report on the aggregation behavior of a model ENP, fullerene nanoparticles (nC₆₀) in the presence of five MW fractions of Suwannee River NOM (M_F-SRNOMs, separated by ultrafiltration techniques) and three electrolytes (NaCl, CaCl₂ and MgCl₂). We found that in all NaCl treatments and low concentration CaCl₂/MgCl₂ treatments, the enhancement of nC₆₀ stability positively correlated with the MW of M_F-SRNOMs. Whereas, the stability efficiency of identical M_F-SRNOM in different electrolytes followed an order of NaCl > MgCl₂ > CaCl₂, and the enhanced attachment of nC₆₀-SRNOM associations was observed in high MW M_F-SRNOM (SRNOM > 100 kD and SRNOM 30–100 kD) at high concentration CaCl₂/MgCl₂. Our results indicate that although the high MW NOM with large humic-like material is the key component for stabilizing nC₆₀ in monovalent electrolyte, it could play a reversed role in promoting the attachment of nC₆₀, especially in long term aggregations and at high concentrations of divalent cations. Therefore, a detailed understanding of the effects of heterogeneous NOM on the aggregation of ENPs should be highly valued, and properly assessed against different cation species and concentrations.

© 2014 Elsevier Ltd. All rights reserved.

* Corresponding author. Tel./fax: +86 10 62849192.

E-mail address: jfliu@rcees.ac.cn (J.-F. Liu).

<http://dx.doi.org/10.1016/j.watres.2014.12.025>

0043-1354/© 2014 Elsevier Ltd. All rights reserved.

1. Introduction

NOM is a poorly defined, complex mixture of molecules with different physical structures, chemical compositions and properties (Chen et al., 2002; Peuravuori and Pihlaja, 1997), and can be regarded as a heterogeneous structure consisting of hydrophobic backbones and hydrophilic side chains (Qu et al., 2010). In aqueous environments, the structure of NOM is closely related to its chemical composition and functional groups, with molecular size, shape and aggregation state considered as key factors influencing physicochemical reactions (Piccolo, 2001; Baalousha et al., 2006). Electrolytes and pH can govern the surface charge and spectroscopic/photochemical properties of NOM in solutions (Her et al., 2003; Christl and Kretzschmar 2001). Furthermore, for di- and multivalent cations, in addition to the electrostatic interaction, interactions such as complexation/cation-bridging effects between functional groups in/among NOM and them, could result in significantly changes of NOM structures as well (Baalousha et al., 2006; Wang et al., 2013; Kloster et al., 2013). It is therefore of environmental significance to understand how the heterogeneous properties of NOM in environmental relevant conditions impact their physicochemical interactions with exogenous substances, especially the engineered nanoparticles (ENPs).

Fullerenes (C_{60}) are among the most widely used ENPs in industry and consumer products (Mauter and Elimelech, 2008). In addition, naturally occurring C_{60} is also widely observed in natural carbonaceous materials (Jehlicka et al., 2005) and combustion process (Murr and Soto, 2005). However, even water treatment plants could not remove all C_{60} . It has been reported that C_{60} in $\mu\text{g L}^{-1}$ range was detected in the effluents of water treatment plants (Farre et al., 2010). Thus, it is predictable that the environmental exposure of C_{60} would be inevitably promoted. Although it has an extremely low water solubility (Jafvert and Kulkarni, 2008), molecular C_{60} can form stable nanoscale aggregates (nC_{60}) in water through solvent-exchange and extended stirring (Brant et al., 2006; Ma and Bouchard, 2009). Despite the low toxicity of nC_{60} to aquatic organisms (Henry et al., 2011) and limited hazard through human exposure (Aschberger et al., 2010), an emerging environmental issue is the role of nC_{60} as a contaminant carrier, which influences the transport, fate and bioavailability of nC_{60} -absorbed contaminants in aqueous environments (Baun et al., 2008). Elucidating the toxicity and risks of nC_{60} requires more detailed studies on its environmental fate and behavior (Lowry et al., 2012; Petosa et al., 2010). This is highly dependent on the size heterogeneity of nC_{60} aggregates in the aqueous environment (Chae et al., 2010), which thus highlights the importance of understanding the aggregation process of nC_{60} .

The inevitable encounter of NOM upon the released nC_{60} and other ENPs in the environment has increased the interest in their active interactions (Lowry et al., 2012; Zhang et al., 2009; Xie et al., 2008). Previous studies have attempted to extend our understanding of ENP interactions with bulk (Zhang et al., 2009) or specific components (Xie et al., 2008; Zhang et al., 2013; Lin and Xing, 2008) of NOM, such as humic acid (HA), fulvic acid (FA) and low-molecular-weight

organic acids. It was observed that nC_{60} could be stabilized in the presence of bulk or specific components of NOM by invoking steric repulsion (Qu et al., 2010; Chen and Elimelech, 2007) resulting from adsorbed NOM layers on nC_{60} . Moreover, FA was found to be less effective than HA as FA has a lower affinity with nC_{60} due to its higher charge density and smaller aromatic backbone (Terashima and Nagao, 2007). In addition, the occurrence of NOM- nC_{60} aggregation may lead to the enhanced aggregation of nC_{60} in solutions with high concentrations of divalent cations (Chen and Elimelech, 2007). It is therefore of significant interest to systematically study how the molecular weight (MW)-dependent physicochemical properties of NOM impact fundamental processes such as the aggregation of nC_{60} , both in the presence and absence of divalent electrolytes. However, to date, only a single study has been reported regarding the influence of simply fractionated NOM (molecular weight >100 kD and <100 kD) on the aggregation behavior of gold nanoparticles in NaCl solutions (Louie et al., 2013). Moreover, to the best of our knowledge, no studies have considered the MW-dependent effects of NOM on the stability of ENPs against different electrolyte species.

The primary objective of this work is to study the effects of MW-dependent physicochemical heterogeneity of NOM on the aggregation kinetics of nC_{60} . To this end, pristine Suwannee River natural organic matter (SRNOM) and isolated MW fractions of SRNOM (M_f -SRNOMs) were comprehensively characterized, and their impacts on nC_{60} aggregation were investigated in monovalent and divalent electrolyte solutions at varying concentrations. Additionally, the adsorption of M_f -SRNOMs onto nC_{60} , surface charge change of nC_{60} , and long term aggregation were fully investigated to assist the discussion. To our knowledge, this is the first study on the impacts of MW distribution and chemical properties' heterogeneity of NOM on the aggregation behavior of nC_{60} in both monovalent and divalent electrolytes.

2. Materials and methods

2.1. Materials

Suwannee River NOM (SRNOM, 1R101N) was obtained from the International Humic Substances Society (St. Paul, MN). C_{60} powder (purity greater than 95%) was obtained from Sigma–Aldrich (St. Louis, MO). All solutions and suspensions were prepared using 18 M Ω cm water produced with a Millipore Milli-Q Gradient system (Billerica, MA). Toluene was obtained from Fisher Scientific (Fair Lawn, NJ). Other reagents were purchased from Sinopharm Chemical Reagent Co. Ltd. (Beijing, China).

2.2. Preparation of pristine and molecular weight fractions of SRNOM

A 500 mg sample of SRNOM was dispersed in 500 mL of deionized water and stirred for 12 h in dark. The solution was then filtered through a 0.45 μm pore-size hybrid fiber membrane to remove any undissolved SRNOM. This filtered solution was referred to as pristine-SRNOM. A molecular weight-based fractionation of pristine-SRNOM was performed using

ultrafiltration techniques with 15 mL centrifugal filter units from Millipore (Billerica, MA) having nominal molecular weight cut-offs (MWCO) of 100, 30, 10 and 3 kD. All filter units were pretreated by rinsing with deionized water to remove residual glycerol. The fractionation of pristine-SRNOM was conducted stepwise with 30 min centrifugation, at 6000–9000 rpm, for each round. Beginning with the highest MWCO, the filtrate was collected and introduced into the cells with a lower MWCO for separation, and the highly concentrated residual solution of higher MW SRNOM fraction was carefully transferred to a vial by pipette. The upper side of membrane on the filter was rinsed with Milli-Q water and the solution was transferred to the vial as well. The MW fractions of SRNOM (collectively referred to as M_f -SRNOMs) obtained from the separation were >100 kD, 30–100 kD, 10–30 kD, 3–10 kD and <3 kD (referred to as SRNOM>100, SRNOM30–100, SRNOM10–30, SRNOM3–10 and SRNOM<3, respectively). All the pristine- and M_f -SRNOM stock solutions were stored in the dark at 4°C until use. The concentration (as carbon) of them was determined using a Teledyne Tekmar Fusion total organic carbon (TOC) analyzer (Mason, Ohio).

2.3. Spectroscopic characterization of pristine- and M_f -SRNOMs

UV–vis spectrophotometric analysis and fluorescence excitation-emission matrices (EEMs) were performed for comprehensively characterizing pristine- and M_f -SRNOMs. Experimental details are given in the [Supplementary Information \(SI\)](#).

2.4. Preparation and characterization of nC_{60} dispersion

The aqueous nC_{60} dispersion was prepared using a modified solvent-exchange method (Xie et al., 2008). Ninety mg C_{60} was added to 90 mL toluene, suspended using a bath sonicator at 600 W for 1 h, and then introduced to 900 mL nitrogen-purged Milli-Q water (toluene/water = 1:10, v/v). The mixture was subsequently shaken for 12 h. The toluene in the mixture was removed by nitrogen purge with sonication at 600 W for 6 h in 25 min cycles with 5 min intervals. The rough suspension was sequentially filtered using 20 μ m, 2 μ m and 0.45 μ m mixed-cellulose-ester membranes. The resulting clear yellow dispersion of nC_{60} was stored in the dark at 4°C until use. The nC_{60} concentration in the stock dispersion, determined by HPLC measurement, was 9.50 mg L⁻¹ (SI). Particle size, morphology and physico-chemical properties of nC_{60} were characterized using a H-7500 transmission electron microscope (TEM, Hitachi, Japan), dynamic light scattering (DLS) and phase analysis light scattering using Malvern ZEN3600 Zetasizer Nano (Worcestershire, UK) and UV–vis spectroscopy (SI). The z-average hydrodynamic radius of nC_{60} was routinely monitored by DLS throughout the duration of the experiments. The detector employed a laser source of 633 nm and detection angle of 173° with each correlation function being accumulated over 10 s by setting the measurement position as 4.65 mm from the bottom and the attenuation as 7, which were the same with DLS test for aggregation process.

2.5. Sorption of pristine- and M_f -SRNOMs by nC_{60}

A one-point batch sorption test was performed to estimate sorption of pristine- and M_f -SRNOMs by nC_{60} . The experiment details are given in SI.

2.6. Electrophoretic mobility measurement

The electrophoretic mobility (EPM) of nC_{60} under various electrolyte solution conditions was measured using a ZEN3600 Zetasizer Nano at 25 °C. Details of the EPM measurements are given in SI.

2.7. Aggregation kinetics of nC_{60} by time-resolved DLS

Time-resolved DLS (TR-DLS) measurements using a ZEN3600 Zetasizer Nano were conducted to investigate aggregation of the nC_{60} dispersion under various solution conditions. The detector employed a laser source of 633 nm and detection angle of 173° with each correlation function being accumulated over 10 s.

The aggregation kinetics of nC_{60} was first tested in three electrolyte solutions without pristine- or M_f -SRNOMs. To investigate the effects of M_f -SRNOMs on nC_{60} aggregation, the pristine- or each M_f -SRNOM solution was added to the nC_{60} dispersion in disposable polystyrene cuvettes (Sarstedt, Germany). Next, monovalent (NaCl) or divalent electrolyte (CaCl₂ or MgCl₂) was added into the cuvette to initiate nC_{60} aggregation. The pH of all samples was adjusted to 7.5 with 1 mmol L⁻¹ appropriate buffers. While phosphate buffer was used in NaCl system, borate buffer was used in CaCl₂ and MgCl₂ systems to avoid the formation of precipitated phosphates. For each sample, the final volume was 1 mL, with 1 mg L⁻¹ nC_{60} and 1 mg C L⁻¹ pristine- or M_f -SRNOM. Details of the TR-DLS measurements, calculation methods for attachment efficiency (α) and critical coagulation concentration (CCC) are given in SI.

2.8. Transmission electron microscopy (TEM) of nC_{60}

Representative TEM images for comparing the morphology of nC_{60} aggregates in the absence and presence of high M_f -SRNOM and divalent electrolyte treatments were captured 4–5 h after the sample prepared and left under the same conditions as in the DLS experiments. Details of the TEM imaging are given in SI.

3. Results and discussion

3.1. Molecular weight distribution of SRNOM

The MW distribution of pristine-SRNOM was evaluated by determining the dissolved organic carbon (DOC) concentration of each M_f -SRNOM isolated from pristine-SRNOM. The carbon weight percent (wt%) of the M_f -SRNOMs collected after ultrafiltration separation was 7.2 for SRNOM>100, 6.6 for SRNOM30–100, 13.0 for SRNOM10–30, 15.5 for SRNOM3–10, and 57.6 for SRNOM<3, yielding 97.0% recovery of the total pristine-SRNOM DOC, indicating the DOC content of the high

MW fraction in SRNOM was much less than the lower MW fraction(s).

3.2. Characterization of pristine- and M_f -SRNOMs

The UV–vis spectra, absorbance at 280 nm (positively correlated to aromaticity) and the E_2/E_3 (absorbance at 250 nm divided by that at 365 nm, inversely correlated to aromaticity) (Peuravuori and Pihlaja, 1997), of 10 mg C L⁻¹ pristine- and M_f -SRNOMs were presented in Fig. 1a–c. Of the five M_f -SRNOMs, SRNOM>100 and SRNOM30–100 had the highest abundance of aromatic components, indicating the aromatic components and more hydrophobic structures existed mainly in higher M_f -SRNOMs. Furthermore, aromaticity decreased consistently with decreasing MW of M_f -SRNOM.

For pristine- and M_f -SRNOMs, fluorescence excitation–emission matrices (Fig. 1d–i) corrected for the inner-filtering effect, showed that the excitation/emission wavelengths (Ex/Em) of spectra peaks in all samples were primarily in the range 345–360/444–464 (Table S1), indicating the presence of humic-like structures (Hudson et al., 2007) in all SRNOMs. Generally, as the MW of the M_f -SRNOMs increased (with the exception of SRNOM>100, probably due to the presence of some relatively large sized but non-humic-like particulates), a detectable red-shift (from 444 to 464) of Em maxima was observed owing to the greater abundance of aromatic chromophores (Wu et al., 2003). Since the humic-like fluorescence is mainly attributed to carboxylic groups (Wu et al., 2003), the general increase in

the fluorescence maxima with decreased MW in the primary peaks of M_f -SRNOM Ex/Em spectra indicates an increased abundance of carboxylic functional groups with decreasing M_f -SRNOM MW. Similar results have also been observed in the MW-fractionation of soil HA (Richard et al., 2007).

3.3. Characterization of nC_{60} nanoparticles

The pristine nC_{60} were spherical-like in shape, with an average diameter of 35.8 nm determined by 257 nC_{60} particles in multi-TEM images (a representative TEM in Fig. S1a and the size distribution of pristine nC_{60} in Fig. S1b) and a z-average hydrodynamic radius of 58.2 nm (polydispersity index (PDI), 0.152), indicating the majority were in well dispersion. The hydrodynamic radius of nC_{60} stock dispersion was routinely measured with DLS throughout the entire experiment period. The limited variations (≤ 2 nm) from the original measurement demonstrated the stability of the nC_{60} stock dispersion, and therefore the reliability of the nC_{60} aggregation results. In addition, the pristine nC_{60} was highly negative charged, with an EPM of -3.6 ± 0.1 $\mu\text{mcm/Vs}$ without electrolytes and -2.8 ± 0.2 $\mu\text{mcm/Vs}$ in 1 mmol L⁻¹ phosphate buffer.

3.4. EPM in the absence and presence of pristine- and M_f -SRNOMs

The EPMs of nC_{60} in the absence of pristine- and M_f -SRNOMs against electrolyte type and concentration were presented in

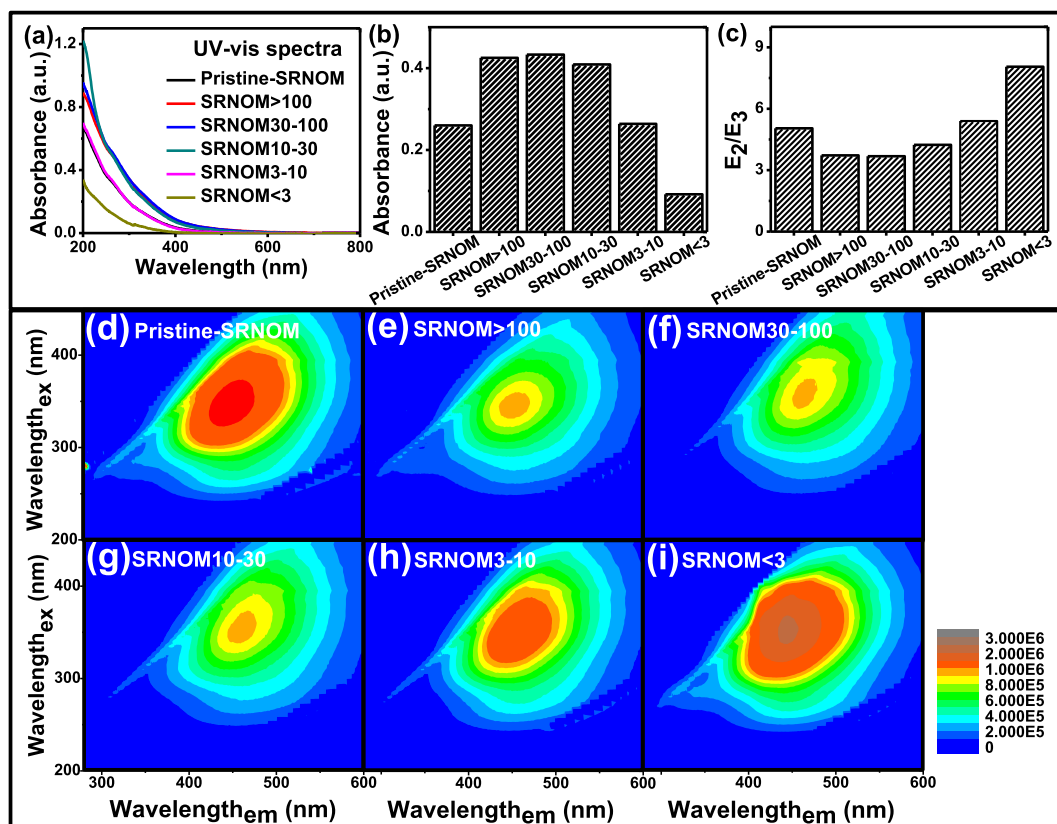


Fig. 1 – (a) UV–vis spectra, (b) the absorbance values at 280 nm and (c) the quotient of absorbance values at 250 nm and 365 nm (E_2/E_3) for pristine- and M_f -SRNOM. Fluorescence EEMs for pristine-SRNOM and M_f -SRNOMs (d–i) (Data in the areas in the top left and bottom right corners where Rayleigh scattering occurs were set to zero).

Fig. S2. The less negative EPM with increasing electrolyte concentrations was ascribed to the charge screening effect, and is consistent with previous studies (Zhang et al., 2013; Chen and Elimelech, 2006). The efficiencies of electrolytes in decreasing EPM followed the order of $\text{CaCl}_2 > \text{MgCl}_2 \gg \text{NaCl}$ due to the more effective attenuation of electrostatic repulsion of divalent cations relative to Na^+ , or the specific adsorption of $\text{Ca}^{2+}/\text{Mg}^{2+}$ to the surface of nC_{60} (Zhang et al., 2013; Chen and Elimelech, 2006).

To facilitate the comparison of the EPM of nC_{60} in reaction-limited and diffusion-limited regimes, representative electrolyte concentrations below and above the CCC value were selected, which are relevant to very hard water, estuarine water and seawater. Fig. 2 shows the EPMs of nC_{60} in the presence of pristine- and M_f -SRNOMs at pH 7.5 and in the presence of NaCl (100 and 500 mmol L^{-1}), CaCl_2 (5 and 20 mmol L^{-1}) and MgCl_2 (5 and 20 mmol L^{-1}), respectively. Generally, the EPM values of nC_{60} strongly depend on the electrolyte concentrations, irrespective of the SRNOM type introduced. Moreover, EPMs varied among the different M_f -SRNOM/electrolyte treatments. One way ANOVA analysis showed that in the 100 and 500 mmol L^{-1} NaCl solutions, EPMs of nC_{60} in the presence of SRNOM>100 and SRNOM30–100 were significantly more negative than those in SRNOM-free solutions (Fig. 2a, Table S2). Whilst this did not hold for the lower M_f -SRNOM (SRNOM3–10 and SRNOM<3), and in general the absolute EPMs correlated positively with MW of the M_f -SRNOMs and were significantly different from each other ($p < 0.05$). The distinctions of EPMs among M_f -SRNOM treatments suggest the adsorption of different quantities of M_f -SRNOM on the surface of nC_{60} . This was confirmed by the sorption of larger amount of higher M_f -SRNOM on nC_{60} surface measured in adsorption experiments (Fig. S3). This is because, the more abundant aromatic components in higher M_f -SRNOMs facilitate their adsorption onto the surface of nC_{60} through hydrophobic and π - π interactions. Similar observation was reported in the sorption of HA and FA to nC_{60} and NOM to C_{60} powder (Zhang et al., 2013; Mashayekhi et al., 2012). As pristine- and M_f -SRNOMs are deprotonated at pH 7.5, the greater adsorption of higher M_f -SRNOM to nC_{60} in turn increased the number of negatively charged functional groups in M_f -SRNOM- nC_{60} association, leading to a more negative EPM. These results reveal the magnitude of M_f -SRNOM adsorption onto nC_{60} , and therefore how the EPM changes

under the different M_f -SRNOM treatments. Such a detailed understanding of M_f -SRNOM influence has not been discovered in previous studies which focus only on a specific type of NOM (Xie et al., 2008; Chen and Elimelech, 2007).

The addition of pristine and M_f -SRNOMs generally had minimal impacts on EPMs of nC_{60} in $\text{Ca}^{2+}/\text{Mg}^{2+}$ solutions (Fig. 2b, c, Table S2). However, it is noteworthy that in the presence of divalent electrolytes, especially CaCl_2 , the adsorption of pristine and M_f -SRNOMs to nC_{60} was much stronger than that in NaCl solutions (or buffer only solutions), with k_d correlating positively with the MW of M_f -SRNOMs (Fig. S3). For Ca^{2+} and Mg^{2+} , the formation constant of humic-like materials with Mg^{2+} is lower than that with Ca^{2+} (Tipping and Hurley, 1992; Akaighe et al., 2012). Therefore, the enhancement of NOM adsorption to nC_{60} by the cations, which followed $\text{Ca}^{2+} > \text{Mg}^{2+} \gg \text{Na}^+$. Given that the $\text{Ca}^{2+}/\text{Mg}^{2+}$ concentrations were significantly higher than carboxylic group contents of pristine- and M_f -SRNOMs (1 mg C L^{-1}), the above results suggests that although the adsorption of pristine- and M_f -SRNOMs to nC_{60} would impart dissociated functional groups on the surface of nC_{60} -SRNOM association, the interactions between divalent cations and negative functional groups would impede the increase of EPMs. Overall, the MW and chemical properties of M_f -SRNOMs drive insignificant change in EPMs of nC_{60} .

3.5. Aggregation kinetics of nC_{60} in the absence of pristine- and M_f -SRNOMs

In 1 mmol L^{-1} phosphate or borate buffer (pH 7.5), the mean hydrodynamic radius of nC_{60} was 60.8 nm after 2 hours of continuous measurement, with a mean PDI of 0.163. This indicates the nC_{60} particles were well dispersed and that no significant aggregation occurred in the 1 mmol L^{-1} buffer solution during the measurement. The aggregation attachment efficiency (α) profiles of nC_{60} in the absence of pristine- and M_f -SRNOM against NaCl, CaCl_2 and MgCl_2 concentration (Fig. S4) clearly delineated reaction-limited and diffusion-limited regimes of nC_{60} aggregation. Extrapolation between the two regimes yielded critical coagulation concentration (CCC) values of 143, 6.2, and 8.0 mmol L^{-1} for NaCl, CaCl_2 and MgCl_2 , respectively, which were comparable with the reported values for nC_{60} prepared by a solvent exchange method (Chen and Elimelech, 2007, 2006; Meng et al., 2013).

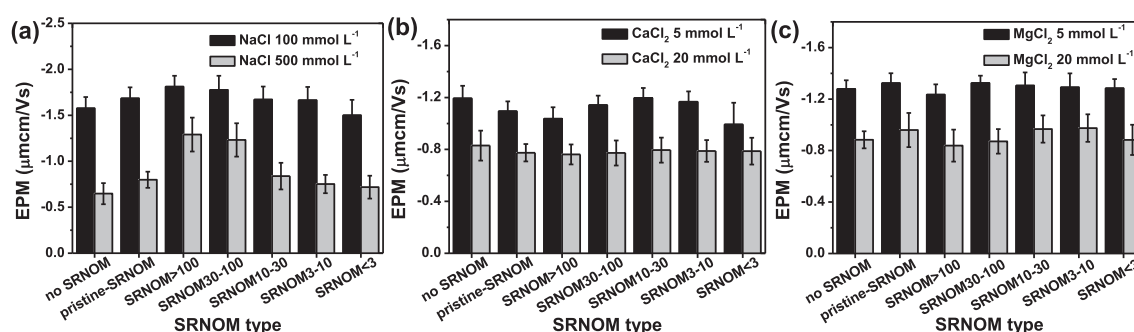


Fig. 2 – EPMs of nC_{60} in the absence and presence of 1 mg C L^{-1} of pristine- and M_f -SRNOMs in representative concentrations of (a) NaCl, (b) CaCl_2 and (c) MgCl_2 solutions. The error bars represent the standard deviation from 6 to 12 measurements of 2–4 samples.

3.6. Aggregation kinetics in the presence of pristine- and M_f -SRNOMs

3.6.1. Stability of nC_{60} in the presence of pristine- and M_f -SRNOMs with NaCl

The effects of pristine- and M_f -SRNOMs on nC_{60} aggregation were first studied with 50–1000 mmol L⁻¹ NaCl (a broad spectrum of natural water types from estuary to sea waters). Representative aggregation profiles of nC_{60} obtained from TR-DLS measurements (500 mmol L⁻¹ NaCl with or without pristine- and M_f -SRNOMs, Fig. 3a) showed that nC_{60} aggregation was suppressed significantly in the presence of a relatively low concentration of pristine- and M_f -SRNOMs (1 mg C L⁻¹). The α values of nC_{60} in the presence of 1 mg C L⁻¹ pristine- and M_f -SRNOMs are plotted as a function of NaCl concentration in Fig. 4. The addition of M_f -SRNOMs resulted in CCC values of 1.06–4.15 times higher than that in SRNOM-free solutions, and the increment of CCC positively correlating to the MW of M_f -SRNOMs. At an identical NaCl concentration in diffusion-limited regimes, pristine- and M_f -SRNOMs generally suppressed α values compared with those for SRNOM-free solutions, and α values were inversely correlated with the MW of the M_f -SRNOMs.

Over the entire NaCl concentration range the attenuation of α values revealed that pristine- and M_f -SRNOMs enhanced the stability of nC_{60} . The right shift of CCC and stronger attenuation of α values in higher M_f -SRNOM treatments also showed that nC_{60} stability positively correlated to the MW of the M_f -SRNOMs. These observations strongly indicated that the steric-hindrance combined with electrostatic effect

(Petosa et al., 2010) was significantly MW-dependent, and was the most important mechanism influencing the stability of nC_{60} in solutions of M_f -SRNOMs/NaCl. In addition, the greater aromaticity in higher M_f -SRNOMs increased their adsorption to nC_{60} , and thus enhanced the nC_{60} stability by providing enhanced negative surface charge and steric hindrance effect.

3.6.2. Suppressed aggregation in the presence of pristine- and M_f -SRNOMs and Low concentrations of $CaCl_2$ or $MgCl_2$

The aggregation kinetics of nC_{60} were also examined in the divalent electrolytes. Fig. 5 shows the α values of nC_{60} as a function of $CaCl_2$ and $MgCl_2$ concentration, respectively. The M_f -SRNOMs suppressed the aggregation of nC_{60} at low $CaCl_2$ and $MgCl_2$ concentrations, similar to that observed for NaCl. Profiles of the stability curves in reaction-limited regimes shifted to the right with an increase in MW of the M_f -SRNOMs. For $CaCl_2$ solutions, CCC values increased with the MW of M_f -SRNOMs from 1.02 to 2.0 times of that in SRNOM-free treatment. For $MgCl_2$ solutions, MW-dependent increase of CCC was observed too, and the CCC in SRNOM > 100 treatment reached to 3.2 times higher than that in SRNOM-free.

These results suggest that M_f -SRNOMs suppressed the aggregation of nC_{60} at low Ca^{2+}/Mg^{2+} concentrations, and indicate the greater stabilization capacity of higher M_f -SRNOM at low divalent electrolyte concentrations. The weakened aggregation of nC_{60} could be attributed to the MW-dependent steric-hindrance effect imparted by the M_f -SRNOM layer. However, a great interest to note in this study is that the right shift of the SRNOM-MW-dependent curves of reaction-limited regimes for $CaCl_2$ was less significant

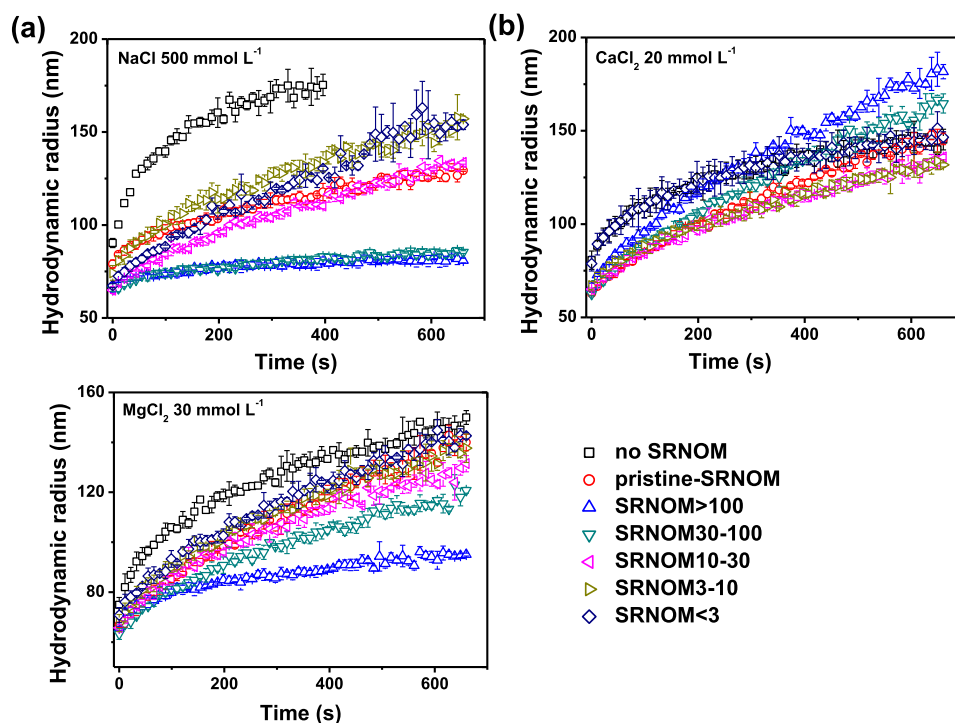


Fig. 3 – Representative aggregation profiles of nC_{60} in the absence and presence of 1 mgC L⁻¹ of pristine- and M_f -SRNOMs at (a) 500 mmol L⁻¹ NaCl; (b) 20 mmol L⁻¹ $CaCl_2$; and (c) 30 mmol L⁻¹ $MgCl_2$. Error bars are standard deviations from triplicate samples at the same solution chemistry. The pH in all treatments was adjusted to 7.5 with 1 mmol L⁻¹ buffer. It should be noted that, although radii data within 11 min were used in this figure, enough radii data ($R_h(t) \geq 1.25R_h(0)$) were recorded for calculation of the initial aggregation rate constant.

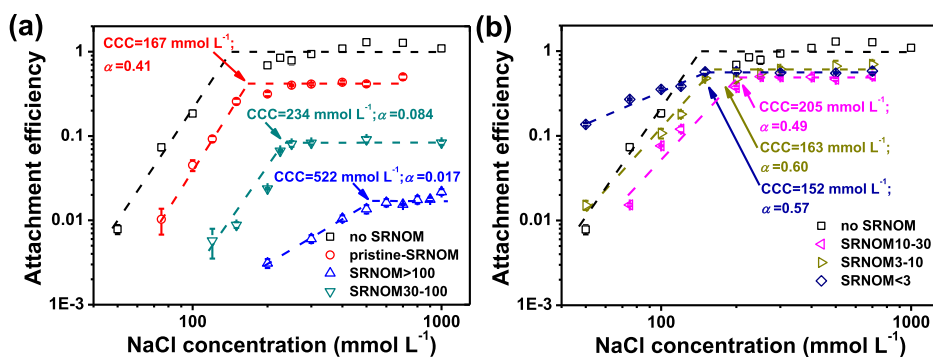


Fig. 4 – Attachment efficiency values of nC_{60} as a function of NaCl concentration in the presence of 1 mg C L^{-1} of pristine- and M_f -SRNOMs. Data for “no SRNOM” (□) solutions are also given (in both a and b) to facilitate comparison of differences in α values among no SRNOM, pristine- and M_f -SRNOM solutions. The error bars represent the standard deviation from triplicate samples. The dashed lines represent a visual guide to distinguish the reaction-limited and diffusion-limited regimes.

than that for $MgCl_2$, and much lesser than that for low NaCl concentrations. The reduction of α values at CCC in identical M_f -SRNOM but different electrolyte treatments followed the same trend too. Therefore, the difference in adsorptions of M_f -SRNOMs to nC_{60} was not the sole reason for the varied efficiency of M_f -SRNOMs in stabilizing nC_{60} against electrolytes. Given the preference of divalent cation binding within the hydrophobic regions of NOM (Engelbreton and von Wandruszka, 1998), and the higher hydrophobicity of higher M_f -SRNOM in our study, it is likely the complexation/cation-bridging between Ca^{2+}/Mg^{2+} and carboxylic functional groups in M_f -SRNOMs preferred to occur in high MW ones. This explains why the cation-induced difference in

stability efficiencies of M_f -SRNOM was more significant in higher M_f -SRNOM treatments.

Overall, the above results suggest that the stabilization effects of M_f -SRNOMs on nC_{60} were dominated by the MW-dependent steric repulsion imparted by the M_f -SRNOMs adsorbed on nC_{60} , while the stabilization efficiency of a specific M_f -SRNOM in different electrolytes followed an order of $NaCl > MgCl_2 > CaCl_2$.

3.6.3. Enhanced attachment in the presence of high M_f -SRNOMs and high concentrations of $CaCl_2$ or $MgCl_2$

In the diffusion-limited regimes of high M_f -SRNOMs/ $CaCl_2$ treatments, enhanced attachment of nC_{60} was observed. The

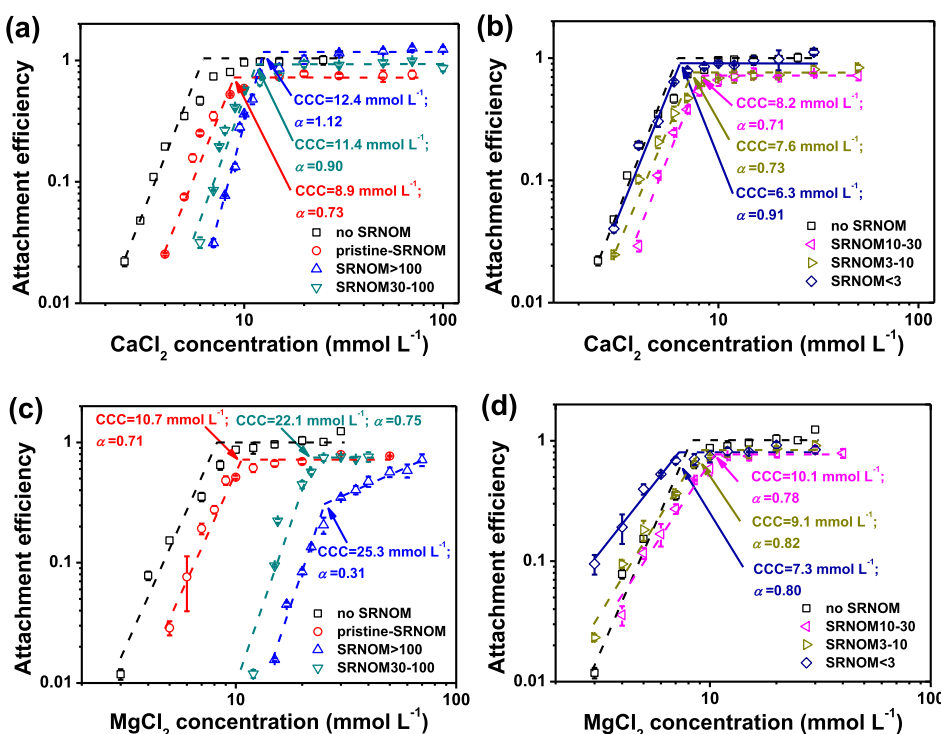


Fig. 5 – Attachment efficiency values of nC_{60} as a function of $CaCl_2$ (a–b), $MgCl_2$ (c–d) concentration in the presence of 1 mg C L^{-1} of pristine- and M_f -SRNOMs. The symbol statements are the same as in Fig. 4.

first evidence was that average α values in SRNOM > 100 and SRNOM 30–100 treatments were greater than those in pristine-SRNOM treatments. This was unlike the behavior observed in the NaCl treatments, where high M_f -SRNOMs suppressed α values significantly more than the pristine-SRNOM did (Figs. 4a and 5a). More noteworthy, an enhanced aggregation ($\alpha = 1.12$) was observed in SRNOM > 100/CaCl₂ treatments. These observations indicated that the coexistence of high M_f -SRNOMs and high Ca²⁺ concentrations could very likely promote the attachment of nC₆₀.

This was further supported by the representative aggregation kinetics profiles of nC₆₀ in the absence and presence of pristine- and M_f -SRNOMs in diffusion-limited regimes at 20 mmol L⁻¹ CaCl₂ (Fig. 3b). As expected, the addition of low M_f -SRNOMs resulted in stabilization of nC₆₀. However, although SRNOM > 100 and SRNOM 30–100 treatments retarded the aggregation of nC₆₀ at the very beginning, they actually accelerated the increase of nC₆₀ hydrodynamic radius in comparison to that in the SRNOM-free treatment over a longer time range (see the differences after 500 s, Fig. 3b). This is further evidenced in the nC₆₀ morphology at approximately 5 h after the initiation of nC₆₀ aggregation in the presence of 20 mmol L⁻¹ CaCl₂ (Fig. 6b, c, f). The z-average hydrodynamic radius increased to 899 nm (PDI, 0.888) for the SRNOM > 100 treatment and 320 nm (PDI, 0.400) for the SRNOM-free treatment, respectively, and condensed shades of SRNOM > 100 aggregates as bridges among nC₆₀ particles in the TEM images were observed. Whereas, light shades of SRNOM < 3 molecular associations could only be observed around the nC₆₀ aggregates, and variations in the hydrodynamic radius and PDI of

nC₆₀ from that determined in SRNOM-free solution were limited (Fig. S5).

The presence of high M_f -SRNOMs and high Mg²⁺ concentrations also promoted the attachment of nC₆₀. A positive-linear-dependent increase of α values was observed with the increase in electrolyte concentration above CCC in SRNOM > 100 treatments. Although the hydrodynamic radii of nC₆₀ in high M_f -SRNOM/MgCl₂ treatments did not exceed any relevant ones in SRNOM-free treatment (Fig. 5c, d), and representative kinetic curves in 30 mmol L⁻¹ MgCl₂ in (Fig. 3c), the DLS results and TEM images for long-term aggregations in 40 mmol L⁻¹ MgCl₂ treatments (Fig. 6d–f) showed that SRNOM > 100 still elevated the hydrodynamic radius and produced some bridges among nC₆₀ aggregates (though less than in SRNOM > 100/CaCl₂ treatment). In contrast, the SRNOM < 3 resulted in a minimal changes of either the morphology or hydrodynamic radii of nC₆₀ when compared with that of the SRNOM-free treatment (Fig. S5).

The enhanced attachment of nC₆₀, especially in long term aggregations, could be attributed to the preferential interaction between Ca²⁺/Mg²⁺ and high M_f -SRNOMs. Previous studies suggested that Ca²⁺/Mg²⁺ preferred to bind within the hydrophobic regions of NOM (Engelbreton and von Wandruszka, 1998), and therefore may attract these NOM fractions toward the hydrophobic regions of the nC₆₀ surface forming more compacted features (Zhang et al., 2013). In addition, very recent studies suggested that Ca²⁺/Mg²⁺ were more effective in enhancing the aggregation of more hydrophobic and aromatic NOM fractions (Wang et al., 2013; Tamamura et al., 2013). Therefore, since higher M_f -SRNOMs

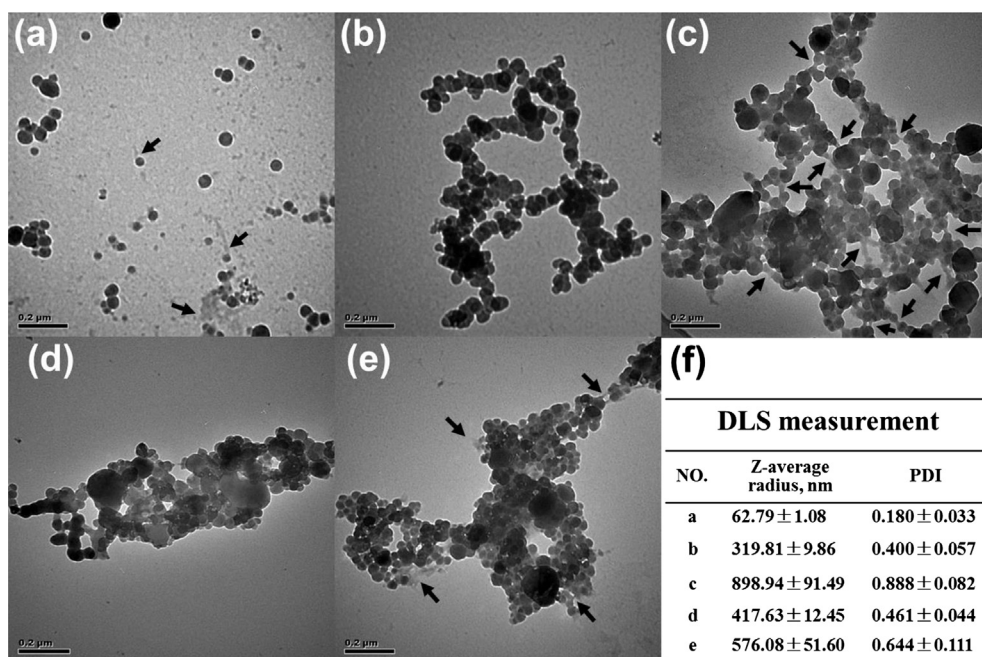


Fig. 6 – Representative TEM images of nC₆₀. (a) nC₆₀ dispersion in the presence of SRNOM > 100 (1 mg C L⁻¹), and nC₆₀ aggregates in (b) SRNOM-free/20 mmol L⁻¹ CaCl₂, (c) SRNOM > 100 (1 mg C L⁻¹)/20 mmol L⁻¹ CaCl₂, (d) SRNOM-free/40 mmol L⁻¹ MgCl₂, (e) SRNOM > 100 (1 mg C L⁻¹)/40 mmol L⁻¹ MgCl₂. (f) Z-average radius and PDI measurements for nC₆₀ aggregates in a–e. The pH in all treatments was adjusted to 7.5 with 1 mmol L⁻¹ borate buffer. All TEM images were captured from samples collected 4–5 h after the initiation of aggregation. Z-average radius and PDI were measured approximately 5 h after the initiation of aggregation (n = 10).

in this study were of higher hydrophobicity and showed greater adsorption to nC_{60} , it is reasonable that at high concentrations of divalent cations, especially Ca^{2+} , the adsorbed SRNOM > 100 and SRNOM30–100 on nC_{60} tended to form more condensed aggregates and engage in bridging nC_{60} aggregates, thus resulting in the greater hydrodynamic radii of nC_{60} –SRNOM associations. As Mg^{2+} has a lower formation constant with humic-like materials than Ca^{2+} (Tipping and Hurley, 1992), and the smaller Mg^{2+} ion (compared to Ca^{2+}) results in an weaker interaction with NOM-coated nanoparticles (Akaighe et al., 2012), the attachment enhancement of nC_{60} in MgCl_2 was thus less significant than in CaCl_2 . However, it should be noted that most initial aggregation rates of nC_{60} in SRNOM/ CaCl_2 (MgCl_2) did not exceed that in CaCl_2 (MgCl_2) only solutions (shown as $\alpha < 1$), confirming that the steric hindrance effect is still operative due to the adsorption of SRNOM onto nC_{60} .

4. Conclusions

In summary, this study has provided an insight into the fate and transport of nC_{60} in aqueous environments, and revealed that (i) NOM showed a clear MW-dependent efficiency on stabilizing nC_{60} in NaCl; (ii) the stability efficiency of identical M_f -SRNOM in different electrolytes followed an order of in $\text{NaCl} > \text{MgCl}_2 > \text{CaCl}_2$; and (iii) although high MW fractions of NOM with large humic-like material act as the most effective components for stabilizing nC_{60} in a monovalent electrolyte (NaCl), they played a reversed role in promoting the attachment of nC_{60} at relatively high concentrations of divalent cations, especially in long term aggregations. It is therefore suggested that a detailed understanding of the effects of heterogeneous NOM on the aggregation of ENPs should be highly valued, and properly assessed against different cation species and concentrations. The study further indicates that ENPs released into high-MW-NOM-abundant waters could be of potential environmental risk since they might ultimately settle to the sediments in estuaries where divalent electrolytes are abundant. Thus, specific conditions in aquatic environments are very likely to influence the distribution of ENPs between the sediment–water interface, which ultimately have impacts on uptake and therefore bioavailability and toxicity of ENPs to aquatic organisms.

Acknowledgments

Strategic Priority Research Program of the Chinese Academy of Sciences (XDB14020101), External Cooperation Program of Chinese Academy of Sciences (GJHZ1206), the National Natural Science Foundation of China (21025729, 21337004), and the Norwegian Research Council (grant number 209685).

Appendix A. Supplementary data

Supplementary data related to this article can be found at <http://dx.doi.org/10.1016/j.watres.2014.12.025>.

REFERENCES

- Akaighe, N., Depner, S.W., Banerjee, S., Sharma, V.K., Sohn, M., 2012. The effects of monovalent and divalent cations on the stability of silver nanoparticles formed from direct reduction of silver ions by Suwannee River humic acid/natural organic matter. *Sci. Total Environ.* 441, 277–289.
- Aschberger, K., Johnston, H.J., Stone, V., Aitken, R.J., Tran, C.L., Hankin, S.M., Peters, S.A.K., Christensen, F.M., 2010. Review of fullerene toxicity and exposure – Appraisal of a human health risk assessment, based on open literature. *Regul. Toxicol. Pharmacol.* 58 (3), 455–473.
- Baalousha, M., Motelica-Heino, M., Le Coustumer, P., 2006. Conformation and size of humic substances: effects of major cation concentration and type, pH, salinity, and residence time. *Coll. Surf. A: Physicochem. Eng. Asp.* 272 (1–2), 48–55.
- Baun, A., Sorensen, S.N., Rasmussen, R.F., Hartmann, N.B., Koch, C.B., 2008. Toxicity and bioaccumulation of xenobiotic organic compounds in the presence of aqueous suspensions of aggregates of nano- C_{60} . *Aquat. Toxicol.* 86 (3), 379–387.
- Brant, J.A., Labille, J., Bottero, J.Y., Wiesner, M.R., 2006. Characterizing the impact of preparation method on fullerene cluster structure and chemistry. *Langmuir* 22 (8), 3878–3885.
- Chae, S.R., Badireddy, A.R., Budarz, J.F., Lin, S.H., Xiao, Y., Therezien, M., Wiesner, M.R., 2010. Heterogeneities in fullerene nanoparticle aggregates affecting reactivity, bioactivity, and transport. *ACS Nano* 4 (9), 5011–5018.
- Chen, K.L., Elimelech, M., 2006. Aggregation and deposition kinetics of fullerene (C_{60}) nanoparticles. *Langmuir* 22 (26), 10994–11001.
- Chen, K.L., Elimelech, M., 2007. Influence of humic acid on the aggregation kinetics of fullerene (C_{60}) nanoparticles in monovalent and divalent electrolyte solutions. *J. Colloid Interface Sci.* 309 (1), 126–134.
- Chen, J., Gu, B.H., LeBoeuf, E.J., Pan, H.J., Dai, S., 2002. Spectroscopic characterization of the structural and functional properties of natural organic matter fractions. *Chemosphere* 48 (1), 59–68.
- Christl, I., Kretzschmar, R., 2001. Relating ion binding by fulvic and humic acids to chemical composition and molecular size. 1. Proton binding. *Environ. Sci. Technol.* 35 (12), 2505–2511.
- Engelbreton, R.R., von Wandruszka, R., 1998. Kinetic aspects of cation enhanced aggregation in aqueous humic acids. *Environ. Sci. Technol.* 32 (4), 488–493.
- Farre, M., Perez, S., Gajda-Schranz, K., Osorio, V., Kantiani, L., Ginebreda, A., Barcelo, D., 2010. First determination of C_{60} and C_{70} fullerenes and N-methylfulleropyrrolidine C_{60} on the suspended material of wastewater effluents by liquid chromatography hybrid quadrupole linear ion trap tandem mass spectrometry. *J. Hydrol.* 383 (1–2), 44–51.
- Henry, T.B., Petersen, E.J., Compton, R.N., 2011. Aqueous fullerene aggregates (nC_{60}) generate minimal reactive oxygen species and are of low toxicity in fish: a revision of previous reports. *Curr. Opin. Biotechnol.* 22 (4), 533–537.
- Her, N., Amy, G., McKnight, D., Sohn, J., Yoon, Y.M., 2003. Characterization of DOM as a function of MW by fluorescence EEM and HPLC-SEC using UVA, DOC, and fluorescence detection. *Water Res.* 37 (17), 4295–4303.
- Hudson, N., Baker, A., Reynolds, D., 2007. Fluorescence analysis of dissolved organic matter in natural, waste and polluted waters – a review. *River Res. Appl.* 23 (6), 631–649.
- Jafvert, C.T., Kulkarni, P.P., 2008. Buckminsterfullerene's (C_{60}) octanol-water partition coefficient (K_{OW}) and aqueous solubility. *Environ. Sci. Technol.* 42 (16), 5945–5950.
- Jehlicka, J., Frank, O., Hamplova, V., Pokorna, Z., Juha, L., Bohacek, Z., Weishauptova, Z., 2005. Low extraction recovery of fullerene from carbonaceous geological materials spiked with C_{60} . *Carbon* 43 (9), 1909–1917.

- Kloster, N., Brigante, M., Zanini, G., Avena, M., 2013. Aggregation kinetics of humic acids in the presence of calcium ions. *Coll. Surf. A: Physicochem. Eng. Asp.* 427, 76–82.
- Lin, D., Xing, B., 2008. Tannic acid adsorption and its role for stabilizing carbon nanotube suspensions. *Environ. Sci. Technol.* 42 (16), 5917–5923.
- Louie, S.M., Tilton, R.D., Lowry, G.V., 2013. Effects of molecular weight distribution and chemical properties of natural organic matter on gold nanoparticle aggregation. *Environ. Sci. Technol.* 47 (9), 4245–4254.
- Lowry, G.V., Gregory, K.B., Apte, S.C., Lead, J.R., 2012. Transformations of nanomaterials in the environment. *Environ. Sci. Technol.* 46 (13), 6893–6899.
- Ma, X., Bouchard, D., 2009. Formation of aqueous suspensions of fullerenes. *Environ. Sci. Technol.* 43 (2), 330–336.
- Mashayekhi, H., Ghosh, S., Du, P., Xing, B., 2012. Effect of natural organic matter on aggregation behavior of C₆₀ fullerene in water. *J. Colloid Interface Sci.* 374, 111–117.
- Mauter, M.S., Elimelech, M., 2008. Environmental applications of carbon-based nanomaterials. *Environ. Sci. Technol.* 42 (16), 5843–5859.
- Meng, Z., Hashmi, S.M., Elimelech, M., 2013. Aggregation rate and fractal dimension of fullerene nanoparticles via simultaneous multiangle static and dynamic light scattering measurement. *J. Colloid Interface Sci.* 392, 27–33.
- Murr, L.E., Soto, K.F., 2005. A TEM study of soot, carbon nanotubes, and related fullerene nanopolyhedra in common fuel-gas combustion sources. *Mater. Charact.* 55 (1), 50–65.
- Petosa, A.R., Jaisi, D.P., Quevedo, I.R., Elimelech, M., Tufenkji, N., 2010. Aggregation and deposition of engineered nanomaterials in aquatic environments: role of physicochemical interactions. *Environ. Sci. Technol.* 44 (17), 6532–6549.
- Peuravuori, J., Pihlaja, K., 1997. Molecular size distribution and spectroscopic properties of aquatic humic substances. *Anal. Chim. Acta* 337 (2), 133–149.
- Piccolo, A., 2001. The supramolecular structure of humic substances. *Soil Sci.* 166 (11), 810–832.
- Qu, X., Hwang, Y.S., Alvarez, P.J.J., Bouchard, D., Li, Q., 2010. UV irradiation and humic acid mediate aggregation of aqueous fullerene (nC₆₀) nanoparticles. *Environ. Sci. Technol.* 44 (20), 7821–7826.
- Richard, C., Guyot, G., Rivaton, A., Trubetskaya, O., Trubetskoj, O., Cavani, L., Ciavatta, C., 2007. Spectroscopic approach for elucidation of structural peculiarities of Andisol soil humic acid fractionated by SEC-PAGE setup. *Geoderma* 142 (1–2), 210–216.
- Tamamura, S., Ohashi, R., Nagao, S., Yamamoto, M., Mizuno, M., 2013. Molecular-size-distribution-dependent aggregation of humic substances by Na(I), Ag(I), Ca(II), and Eu(III). *Coll. Surf. A: Physicochem. Eng. Asp.* 434, 9–15.
- Terashima, M., Nagao, S., 2007. Solubilization of [60]fullerene in water by aquatic humic substances. *Chem. Lett.* 36 (2), 302–303.
- Tipping, E., Hurley, M.A., 1992. A unifying model of cation binding by humic substances. *Geochim. Cosmochim. Acta* 56 (10), 3627–3641.
- Wang, L.-F., Wang, L.-L., Ye, X.-D., Li, W.-W., Ren, X.-M., Sheng, G.-P., Yu, H.-Q., Wang, X.-K., 2013. Coagulation kinetics of humic aggregates in mono- and di-valent electrolyte solutions. *Environ. Sci. Technol.* 47 (10), 5042–5049.
- Wu, F.C., Evans, R.D., Dillon, P.J., 2003. Separation and characterization of NOM by high-performance liquid chromatography and on-line three-dimensional excitation emission matrix fluorescence detection. *Environ. Sci. Technol.* 37 (16), 3687–3693.
- Xie, B., Xu, Z.H., Guo, W.H., Li, Q.L., 2008. Impact of natural organic matter on the physicochemical properties of aqueous C₆₀ nanoparticles. *Environ. Sci. Technol.* 42 (8), 2853–2859.
- Zhang, Y., Chen, Y.S., Westerhoff, P., Crittenden, J., 2009. Impact of natural organic matter and divalent cations on the stability of aqueous nanoparticles. *Water Res.* 43 (17), 4249–4257.
- Zhang, W., Rattanadompol, U.S., Li, H., Bouchard, D., 2013. Effects of humic and fulvic acids on aggregation of aqu/nC₆₀ nanoparticles. *Water Res.* 47 (5), 1793–1802.